

DAA/LANGLEY

Semi-Annual Status Report  
Period 10/1/86 - 3/31/87

IN-09

64469 - R

P. 27

Implementation and Validation of a Wake Model for Vortex-Surface Interactions  
in Low Speed Forward Flight

Narayanan M. Komerath (Principal Investigator)  
Olivier A. Schreiber (Graduate Research Assistant)  
School of Aerospace Engineering  
Georgia Institute of Technology  
Atlanta, Georgia

(NASA-CR-180623) IMPLEMENTATION AND  
VALIDATION OF A WAKE MODEL FOR  
VORTEX-SURFACE INTERACTIONS IN LOW SPEED  
FORWARD FLIGHT Semiannual Status Report, 1  
Oct. 1986 - 31 Mar. (Georgia Inst. of Tech.)

N87-26923

Unclas  
63/09 0064469

Prepared for  
NASA Langley Research Center  
Under Research Grant No. NAG-1-693  
March 1987

# Implementation and Validation of a Wake Model for Vortex-Surface Interactions in Low-Speed Forward Flight.

## Background

.During the crucial phases of vertical take-off, hovering, and low-speed forward flight, rotary wing aircraft operate in a flowfield which is significantly affected by the wake of the rotor blades. The predominant feature of this wake is the presence of strong vortices shed from the blade tips, which then take an approximately helical trajectory, skewed by the motion of the craft. The close proximity of these vortices to one another and to the rotor blades can significantly modify the performance of the vehicle. To predict the performance of rotorcraft, therefore, one must be able to compute the velocity field induced by the tip vortices. This is a computationally expensive task, since the contributions of every element of the vortex shed from each blade to the velocity at each point of interest must be considered, as well as mutual and self-induced contributions of the vortices themselves. For a practical rotorcraft configuration, with several rotor blades and complex airframes, such computations can be prohibitively expensive.

Beddoes (1) showed that the velocity induced by a helical vortex trajectory at a point was dominated by contributions due to vortex elements positioned at certain "critical" orientations with respect to the point. The remainder of the vortex trajectory contributed very little, and the time spent in computing these contributions was essentially wasted. Thus he approximated each turn of the helical trajectory by two straight line vortex elements positioned at critical locations, plus a "remainder" term to account for the rest of the spiral. The savings in computer time were dramatic, and Beddoes claimed that excellent agreement with observed data could be achieved. Beddoes' interest, however, was aimed at the loads on the rotor blade itself due to close blade-vortex interactions.

It was proposed by the author of this report that this method could be extended to several useful cases, such as those where the influence of an airframe has to be iteratively computed. In addition, other applications have since been identified, such as the rapid computation of the induced velocity field above and below the rotor, identification and interpretation of experimentally observed features, and the validation of more sophisticated blade flowfield codes (such as Navier-Stokes formulations) which require the coupling of some form of wake model to produce results which can be compared with experiment. This work has since been undertaken, and forms the subject of this report.

## Objectives

The objectives for the current year are:

- (1) to code and implement Beddoes' wake model in a VAX workstation environment,
- (2) use the code to perform predictions of induced velocity at specified points of a rotor wake in forward flight  
and
- (3) compare the results to those obtained using the Scully free wake code.

As permitted by time, it is also planned to extend the code to enable calculation of vortex-induced effects on an airframe model and compare the predictions to experimental data.

#### Status Summary at the end of six months

The wake model has been implemented using a VAX 750 and a Microvax II workstation. Online graphics capability is available using a DISSPLA graphics package. The results shown in the paper by Beddoes have been reproduced satisfactorily. The rotor model used by Beddoes has been significantly extended to include azimuthal variations due to forward flight and a simplified scheme for locating critical points where vortex elements are placed. The procedure for computing the remainder term has been modified to remove discontinuities which became apparent when the results were plotted over the rotor disk. The procedure has also been extended to enable computation of velocity at points off the rotor blade, and then to enable computation of time-resolved and time-averaged velocity at fixed points in the flowfield. The current computation procedure has been detailed by Olivier Schreiber in Appendix A, and some of the latest results have been shown.

A test case has been obtained from current NASA work<sup>(2)</sup> for validation of the predictions of induced velocity. Comparison of results indicates that the code requires some more features before satisfactory predictions can be made over the whole rotor disk. Specifically, shed vorticity due to the azimuthal variation of blade loading must be incorporated into the model. Interactions between the vortices shed from the four blades of the model rotor must be included. These modifications are being implemented.

The Scully code for calculating the velocity field is being modified in parallel with these efforts to enable comparison with experimental data. To-date, some comparisons with flow visualization data obtained at Georgia Tech have been performed, and show good agreement for the isolated rotor case. Comparison of time-resolved velocity data obtained at Georgia Tech also shows good agreement. Modifications are being implemented to enable generation of time-averaged results for comparison with NASA data. The efforts to-date on the Scully code have been performed under ARO support as part of the research on rotor-body interactions, and has not to-date been supported under this grant. However, during the next reporting period, the validated Scully code will be used for comparison with NASA results and the Beddoes model will be incorporated into the Scully code.

During the next reporting period, efforts will be concentrated on improving the modeling of the wake and the rotor. Two test cases are available for validation: the NASA data, and the data being acquired at Georgia Tech. Both will be used. The code will be revised and updated periodically as changes are made and validated. With the campus network reaching completion, it is expected to become a routine matter to transmit data and code between Langley and Tech. Some such transmissions have been made already.

#### Extended Work

Quantitative flow visualization data recently obtained at Georgia Tech now promise to enable modeling and validation of vortex-surface interaction phenomena, as discussed in the "extended work" portion of the proposal. This will be attempted in the next reporting period. In addition, there is considerable interest in computing wake effects efficiently to enable accurate

flowfield predictions in the close vicinity of the blade using more sophisticated rotor aerodynamics formulations<sup>(3)</sup>. These avenues are being explored.

#### References

1. Beddoes, T.S., "A Wake Model for High Resolution Airloads". Presented at the First International Conference on Rotorcraft Basic Research, Research Triangle Park, North Carolina, February 1984.
2. Berry, J.D., Hoad, D.R., Helliott, J.W., and Althoff, S.L., "Helicopter Rotor Induced Velocities: Theory and Experiment". Presented at the AHS Specialists' Meeting on Aerodynamics and Aeroacoustics, Arlington, Texas, February 25-27, 1987.
3. Wake, B.E., and Sankar, L.N., "Solutions of the Navier-Stokes Equations for the Flow About a Rotor Blade". Presented at the AHS Specialists' Meeting on Aerodynamics and Aeroacoustics, Arlington, Texas, February 25-27, 1987.

FINANCIAL SUMMARY

<u>Category</u>	<u>Percent Expended or Encumbered</u>
Salaries & Wages	50%
Benefits	50%
Supplies	0%
Travel	0%
Overhead	50%

# Computation of induced velocities

Olivier A. Schreiber

March 16, 1987

This report shows the computer implementation of the calculations of the induced velocities produced by a wake model presented in *A wake model for high resolution airloads* by T.S. Beddoes.<sup>1</sup>(Reference [1])

## Abstract

An implementation of a trailing vortex system geometry is developed. It is combined with a new approach to compute the induced downwash. The program development includes added features in addition to the wake model presented in reference [1]: Circulation harmonic variation possibilities, simplified algorithm for the location of the critical elements of the wake, computation of downwash outside of the blade and/or outside the tip path plane, possibility of including blade bound vorticity induced velocity with harmonic circulation variation. In addition to the computation of induced velocities with wake fixed at a given time, a time averaging process over a rotor revolution divided by the number of blades is carried out. Thus, results can be compared to experimental field measurements obtained in reference [5]. Various options and parameters' influence on the results can be investigated in the future and may allow the model to give useful results for comparison with experimental data.

## 1 Notation

- $a_{0c}$  Zeroth harmonic coefficient for the bound circulation
- $a_{1c}$  First harmonic, longitudinal, for the bound circulation
- $b_{1c}$  First harmonic, lateral, for the bound circulation
- $b$  Number of blades
- $c$  Blade chord
- $c'$  Blade chord, normalized w.r.t.  $R$
- $c_c$  Vortex core radius, normalized w.r.t.  $c$

---

<sup>1</sup>Westland Helicopters Ltd.

- $c_R$  Vortex core radius, normalized w.r.t.  $R$  ( $c_R = c_c c'$ )
- $C_T$  Thrust coefficient  $T/(\rho\pi R^4\Omega^2)$
- $i_{blade}$  Blade index ( range: 1 to  $b$  )
- $i_N$  Spiral turn index ( range: 1 to  $N$  )
- $\vec{i}$  unit vector parallel to tip path plane and to the vertical plane containing the freestream velocity
- $\vec{i}_{AC}$  unit tangent vector to the spiral at a given point, ( $\vec{i}_{AC} = (d\vec{O}m/d\Delta\psi_v)/\|d\vec{O}m/d\Delta\psi_v\|$ )
- $\vec{j}$  unit vector parallel to tip path plane and such that  $\vec{j} = \vec{k} \times \vec{i}$ .
- $\vec{j}_{AC}$  unit normal vector to the spiral at a given point, ( $\vec{j}_{AC} = \vec{k} \times \vec{i}_{AC}$ )
- $\vec{k}$  unit vector perpendicular to the tip path plane and directed upward.
- $N$  Number of spiral turns used
- $p_B$  projection of vector  $\vec{P}B$  on  $\vec{j}_{AC}$  ( $p_B = \vec{P}B \cdot \vec{j}_{AC}$ )
- $r_p$  Radial coordinate of point P, where the induced velocity is being computed non dimensional w.r.t.  $R$
- $r_v$  Contracted radius, non dimensional w.r.t.  $R$
- $R$  Rotor radius
- $\mathcal{R}$  Algebraic curvature radius of projected spiral in tip path plane
- $T$  Rotor thrust
- $v$  Induced velocity (positive up)
- $V$  Free stream velocity
- $x, y, z$  Coordinates of a point in the  $\vec{i}, \vec{j}, \vec{k}$  vector base.
- $z_{PB}$ :  $z$  ordinate difference between point P and point B. ( $z_{PB} = \vec{k} \cdot \vec{P}B/R = z_B - z_P = z_v - z_P$ )
- $\alpha$  Angle of attack, rotor tip path plane (negative in forward flight)
- $\alpha$  Radial abscissa integration variable
- $\beta$  Angle between vortex segment and blade of reference ( $\beta = \Phi_v - \psi_P$ )
- $\beta$  Integration variable
- $\Delta\psi_v$  age of a vortex line point.

- $\Gamma$  Circulation strength
- $\Gamma'$  Normalized circulation strength ( $\Gamma/(R^2\Omega)$ )
- $\Gamma_{eff}$  Corrected circulation strength with respect to vortex core model
- $\kappa$  Wake skew angle,  $(-\tan^{-1}(\mu_x/\lambda))$
- $\lambda$  Inflow ratio,  $(\mu_z + \lambda_i)$ , positive up.
- $\lambda_i$  Induced inflow ratio,  $(v/\Omega R)$
- $\lambda_i^*$  Reduced induced inflow ratio,  $(\lambda_i/\lambda_{i0H})$
- $\lambda_{i0}$  Momentum value of induced inflow ratio
- $\lambda_{i0H}$  Momentum value of induced inflow ratio at hover  $(-\sqrt{C_T/2})$
- $\mu_x$  Advance ratio,  $(V \cos \alpha/\Omega R)$  in tip path plane reference frame
- $\mu_z$  Complementary ratio,  $(V \sin \alpha/\Omega R)$  in tip path plane, reference frame, negative in forward flight or climb.
- $\Omega$  Rotor rotational velocity
- $\Phi_v$  Azimuth angle of straight vortex line segment ( $\Phi_v = \arg \vec{i}_{AC}$ )
- $\psi_r$  Azimuth angle of reference blade
- $\psi_b$  Azimuth angle of blade of index  $i_{blade}$
- $\psi_P$  Azimuth angle of point P where the induced velocity is computed
- $\rho$  Radial distance from vortex center / core radius
- $\rho$  Air density, where appropriate
- $\sigma$  Rotor solidity,  $(bc/\pi R)$

## 2 Introduction

A wake model for high resolution airloads (Reference [1]) showed that the problem of determining the induced downwash through a rotor at low advance ratios can be solved in two successive steps: First, a geometric model of the distorted trailing vortex system of the wake is defined and computed from a prescribed time averaged downwash distribution. Then, the induced velocity is evaluated by positioning simple straight vortex segments at critical locations in the wake with respect to the point where the induced velocity is computed and adding a remainder term to account for the neglected portions of the wake. The computation time of the induced velocity at a given point can thus be divided in

two parts: The location of the critical positions of the wake (two for each spiral turn), and the three terms making up the induced velocity for each spiral turn (a straight vortex segment for each of the two positions and a remainder term). The advantage of this approach is decreased computation time compared to a classical approach scheme where each spiral turn is broken down in small straight vortex segments which location must also be computed.

An induced velocity computation is characterized by: One point P where the induced downwash is wanted, the rotor position at a certain time as given by the azimuth angle of a reference blade  $\psi_r$ . It is possible, then, to compute the downwash seen by a blade at a given azimuth if point P is ascribed to lay on the blade. It is also possible to compute the induced downwash at a point outside the blade and even outside the tip path plane when the rotor is at a particular position defined by  $\psi_r$ . However, to compare induced downwash computed through numerical models with those measured at experimental facilities, it is necessary to perform a time averaging process: The induced downwash at a point in the field is computed by placing point P at this point and then compute the induced downwash for different positions of the rotor at successive increments of azimuth  $\psi_r$  until the rotor has assumed the same orientation in the sense of the computation. In effect, the rotor completes one revolution divided by the number of blades  $b$ . As a result, the model has been adapted for the computation of induced downwash outside the blade and/or outside the tip path plane. This, in turn, necessitated simplification of the algorithm to compute the location of the critical locations of the trailing vortex system. A discontinuity inherent to the former method was thus removed, and with it, an extra remainder term, necessary to iron out that spurious effect. A first harmonic variation of circulation has been added to represent the variation of circulation strength along the tip vortex turns. However, consistency would require inclusion of a shed vortex system to assure vortex continuity. A first step in this direction has been added in the form of the bound circulation induced velocity from the blades. Further study of the model in its present state will yield the influence and relative importance of the various options and parameter variations available to see whether approximation of experimental results by the model can be obtained.

### 3 General description of the wake model

The wake modeled here is the trailing vortex system only. The shed wake is not part of the model. The trailing wake is represented by effectively rolled up tip vortex lines trailed by each blade from effective vortex radial sources at location  $r_v$ , contracted radius. Each of these spiral-like lines follow a cylinder skewed according to the advance ratio. The model defines the geometry of those lines and then computes the induced velocities by approximating each spiral turn by a pair of large straight vortex segments positioned at critical points relative to

where the induced velocity is wanted. A remainder term for the rest of the spiral term is then added. A finite core model is used for the computations as well as a radial averaging of the computed downwash for which a realistic sample is wanted on a blade.

## 4 Description of the wake tip vortex line geometry

A prescribed geometry presented in reference [3] is used. The vertical displacement of elements of the wake is computed by integration of a prescribed time averaged downwash field given in reference [2]. The tip vortex lines are parametrically represented with coordinates  $x_v$ ,  $y_v$ ,  $z_v$  in the tip path plane frame of reference moving with the rotor. The parameters are:

1.  $i_{blade}$  or the index of the blade from which the given vortex line trails ( range: 1 to  $b$  )
2.  $\psi_p$  the angular position of the reference rotor blade ( $i_{blade} = 1$ ) ( range: 0 to one turn )
3.  $\Delta\psi_r$  the age of a vortex line element. It is defined as the angle by which the rotor has turned since that element was produced. ( range: 0 to a  $N$  number of turns )

Thus,

$$\left\{ \begin{array}{l} x_v = r_v \cos \psi_v + \mu_x \Delta\psi_v \\ y_v = r_v \sin \psi_v \\ z_v = \int_0^{\Delta\psi_r} \lambda d\psi \end{array} \right\} \quad (1)$$

with

$$\psi_v = \psi_r + 2\pi(i_{blade} - 1)/b - \Delta\psi_v \quad (2)$$

It follows from the definition  $\lambda = \mu_z + \lambda_i$  that

$$z_v = \mu_z \Delta\psi_v + \int_0^{\Delta\psi_r} \lambda_i d\psi \quad (3)$$

The averaged downwash field, within the disc defined by the contracted radius  $r_v$  is given by:

$$\lambda_i = \lambda_{i0}(1 + Ex' - E|y'^3|) \quad (4)$$

where primed values are normalised by  $r_v$  and  $E = |\kappa|$ . To the rear of the disc, the averaged downwash field is given by:

$$\lambda_i = 2\lambda_{i0}(1 - E|y'^3|) \quad (5)$$

Here,  $\lambda_{i0}$  is the momentum theory value of the induced inflow ratio and is the solution of:

$$-\frac{C_T}{2\lambda_{i0}} = [(\mu_z + \lambda_{i0})^2 + \mu_z^2]^{\frac{1}{2}} \quad (6)$$

Three cases present themselves:

1.  $\cos \psi_v > 0$  The vortex element has always been at the rear of the disc.

$$z_v = \mu_z \Delta \psi_v + 2\lambda_{i0} \int_0^{\Delta \psi_v} (1 - E|y'^3|) d\psi$$

$$z_v = \mu_z \Delta \psi_v + 2\lambda_{i0} (1 - E|y'^3|) \Delta \psi_v \quad (7)$$

2.  $\cos \psi_v < 0$ ,  $x_v < -r_v \cos \psi_v$  The vortex element has not moved beyond the disc. Thus:

$$z_v = \mu_z \Delta \psi_v + \lambda_{i0} \int_0^{\Delta \psi_v} (1 + E x' - E|y'^3|) d\psi$$

$$z_v = \mu_z \Delta \psi_v + \lambda_{i0} \int_0^{\Delta \psi_v} (1 + E(\cos \psi_v + \mu_x \Delta \psi_v / r_v) - E|y'^3|) d\psi$$

$$z_v = \mu_z \Delta \psi_v + \lambda_{i0} (1 + E(\cos \psi_v + \mu_x \Delta \psi_v / (2r_v) - |y'^3|)) \Delta \psi_v \quad (8)$$

3.  $\cos \psi_v < 0$ ,  $x_v > -r_v \cos \psi_v$  The vortex element has spent part of the time within the disc and the remainder to the rear of the disc; thus:

$$z_v = \mu_z \Delta \psi_v + \lambda_{i0} \int_0^{\Delta \psi_{v1}} (1 + E x' - E|y'^3|) d\psi + 2\lambda_{i0} \int_{\Delta \psi_{v1}}^{\Delta \psi_v} (1 - E|y'^3|) d\psi$$

where  $\Delta \psi_{v1} = -2r_v \cos \psi_v / \mu_x$  thus:  $z_v = \mu_z \Delta \psi_v + \lambda_{i0} (1 + E(\cos \psi_v + \mu_x (-2r_v \cos \psi_v / \mu_x) / (2r_v) - |y'^3|)) (-2r_v \cos \psi_v / \mu_x) + 2\lambda_{i0} (1 - E|y'^3|) (\Delta \psi_v + 2r_v \cos \psi_v / \mu_x)$  which simplifies to:

$$z_v = \mu_z \Delta \psi_v + 2\lambda_{i0} (1 - E|y'^3|) x_v / \mu_x \quad (9)$$

## 5 Computation of induced velocities

For each spiral turn, the vortex lines trailed by each blade are accounted for, in the computation of induced velocity by placing a pair of straight vortex segments at critical locations, and adding a remainder term. In this model, the vortex lines have constant circulation estimated from the the total thrust. In consistency with the simplicity of the model, the computation of the induced velocity by the bound vorticity of each blade is easily added as constant circulation straight vortex segments of length equal to the contracted radius. In case the distribution of downwash is wanted along the blade, reference [1] presents a radially averaged downwash expression. The radial definition interval used to sample the distribution is the length used for averaging.

## 5.1 Pair of vortex segments

For a given point P where the induced velocity is needed, and for each spiral turn of each vortex line, two points B are positioned to support a straight vortex segment of length  $2r_v$  and circulation  $\Gamma_{eff}$ . The segments are horizontal (i.e. oriented parallel to the tip path plane) and are such that their projection on the tip path plane is tangent to the projected spiral in the tip path plane. The point of tangency is the point for which the normal to the projected spiral passes through the projected point of P in the tip path plane. By convention, B is the point having the closest projection point to the projection of P in the tip path plane. The induced velocity induced by, say segment AC, placed at B, at point P can be computed as follows:

$$v_B = \vec{k} \frac{\Gamma_{eff}}{4\pi} \int_{M=A}^{M=C} \frac{d\vec{l} \times \vec{M}P}{\|\vec{M}P\|^3} \quad (10)$$

where  $\vec{k}$  is the unit vector perpendicular to the tip path plane and directed upward,  $d\vec{l} = dl \vec{i}_{AC} = R d\alpha \vec{i}_{AC}$ , where  $\vec{i}_{AC}$  is the unit tangent vector to the projected spiral at point B obtained in the following way:

$$\vec{i}_{AC} = \frac{\frac{d\vec{O}m}{d\Delta\psi_v}}{\left\| \frac{d\vec{O}m}{d\Delta\psi_v} \right\|}$$

where  $\vec{O}m = x_v \vec{i} + y_v \vec{j}$ . From (1), we obtain:

$$\frac{d\vec{O}m}{d\Delta\psi_v} \begin{pmatrix} r_v \sin \psi_v + \mu_z \\ -r_v \cos \psi_v \\ 0 \end{pmatrix} \quad (11)$$

Defining  $\vec{j}_{AC}$  unit normal vector to the spiral at point B, directed outward the concavity as

$$\vec{j}_{AC} = -\frac{\frac{d\vec{i}_{AC}}{d\Delta\psi_v}}{\left\| \frac{d\vec{i}_{AC}}{d\Delta\psi_v} \right\|}$$

we see that for advance ratios smaller than 1, there is no inflexion point on the spirals and thus  $\vec{j}_{AC}$  is also:

$$\vec{j}_{AC} = \vec{k} \times \vec{i}_{AC}$$

$\Gamma_{eff}$ , in algebraic value along the orientation  $\vec{i}_{AC}$  is given in the form based on reference [4],

$$\Gamma_{eff}(\rho) = \Gamma \left( \frac{\rho^2}{1 + \rho^2} \right) \quad (12)$$

and

$$\Gamma = \Gamma_0 (1 - a_{1c} \cos \psi_v - b_{1c} \sin \psi_v) \quad (13)$$

where  $\rho$  is the ratio between radial distance and core radius. Reference 1 suggests a constant circulation strength given here in non-dimensional form:

$$\Gamma'_0 = \frac{\Gamma_0}{R^2\Omega} = a_{0c}\pi\frac{C_T}{b} \quad (14)$$

with  $a_0 = 2.4$  Now, projecting  $\vec{M}P$  on the  $\vec{i}_{AC}, \vec{j}_{AC}, \vec{k}$  vector base,

$$\vec{M}P = \vec{M}B - Rz_{PB}\vec{k} - Rp_B\vec{j}_{AC}$$

where  $z_{PB} = \vec{k}\cdot\vec{P}B/R = z_B - z_P = z_v - z_P$ ,  $p_B = \vec{P}B\cdot\vec{j}_{AC}$ . Then,  $\vec{M}P = -R\alpha\vec{i}_{AC} - Rz_{PB}\vec{k} - Rp_B\vec{j}_{AC}$  then,  $d\vec{l} \times \vec{M}P = dlR(z_{PB}\vec{j}_{AC} - p_B\vec{k})$  and  $\vec{k}(d\vec{l} \times \vec{M}P) = -Rp_Bdl = -R^2p_Bd\alpha$ . Also, we have  $(\vec{M}P)^2 = (\alpha^2 + z_{PB}^2 + p_B^2)R^2$  thus:

$$v_B = -\frac{\Gamma'_{eff}}{4\pi R} \int_{\alpha=-r_v}^{\alpha=+r_v} \frac{p_B d\alpha}{(\alpha^2 + z_{PB}^2 + p_B^2)^{3/2}}$$

Switching to non-dimensional variables  $v'_B = v_B/(R\Omega)$ ,  $\Gamma'_{eff} = \Gamma_{eff}/(R^2\Omega)$ , we obtain:

$$v'_B = -\frac{\Gamma'_{eff}p_B}{4\pi} \int_{\alpha=-r_v}^{\alpha=+r_v} \frac{d\alpha}{(\alpha^2 + z_{PB}^2 + p_B^2)^{3/2}}$$

With  $\beta^2 = z_{PB}^2 + p_B^2$  and  $\sinh\theta = \frac{\alpha}{\beta}$ , we obtain

$$v'_B = -\frac{\Gamma'_{eff}p_B}{2\pi\beta^2} \int_0^{\arg\sinh(\frac{r_v}{\beta})} \frac{d\theta}{\cosh^2\theta}$$

$$v'_B = -\frac{\Gamma'_{eff}p_B}{2\pi\beta^2} \tanh(\arg\sinh(\frac{r_v}{\beta}))$$

$$v'_B = -\frac{\Gamma'_{eff}p_B}{2\pi\beta^2} \frac{1}{\sqrt{1 + (\frac{\beta}{r_v})^2}}$$

Thus, we finally have the expression  $v'_B$ :

$$v'_B = -\frac{\Gamma'_{eff}r_v p_B}{2\pi(z_{PB}^2 + p_B^2)} \frac{1}{(z_{PB}^2 + p_B^2 + r_v^2)^{1/2}} \quad (15)$$

with  $\Gamma'_{eff} = \Gamma'(\frac{\rho^2}{1+\rho^2})$  and  $\rho^2 = \frac{(p_B^2 + z_{PB}^2)}{c_R^2}$

## 5.2 Remainder term

The remainder term accounts for the contribution of the remaining portion of the spiral turn. Reference 1 provides the following approximate expression, where B represents the closest proximity of the spiral turn to point P:

$$v'_R = -\Gamma'_{eff}r_v \frac{0.275}{(p_M^2 + z_{PB}^2 + (1 - p_B/r_v)z_{PB})(1 + z_{PB}^2)^{1/2}} \quad (16)$$

with  $\Gamma'_{eff} = \Gamma'(\frac{\rho^2}{1+\rho^2})$  and  $\rho^2 = \frac{(p_M^2 + z_{PB}^2)}{c_R^2}$  where  $p_M = 1 - p_B/r_v$  if  $P$  is outside the concavity or  $p_M = 1$  if  $P$  is inside the concavity (i.e., according to whether  $P_B$  is negative or positive, respectively.)

### 5.3 Blade bound vorticity

The blades bound vorticity contributions to the induced velocity computed at a point  $P$  are computed in the form of straight vortex segments of length  $r_v$ , along the blades of the rotor. In the tip path plane frame of reference, with origin at the center  $O$  of the rotor, the points  $O$ , and  $P$  have the coordinates  $O : (0, 0, 0)$ ,  $P : (Rx_P, Ry_P, Rz_P)$  and for a blade of index  $i_{blade}$ , the extremity  $C$  of the straight vortex segment assigned to it has the normalized coordinates  $x_C = r_v \cos \psi_b$ ,  $y_C = r_v \sin \psi_b$  and  $z_C = 0$  where  $\psi_b = \psi_r + 2\pi(i_{blade} - 1)/b$ . The induced velocity induced by segment  $OC$  can be computed as follows:

$$v_{i_{blade}} = \vec{k} \frac{\Gamma'_{eff}}{4\pi} \int_{M=O}^{M=C} \frac{\vec{dl} \times \vec{MP}}{\|\vec{MP}\|^3} \quad (17)$$

Now,  $\vec{MP} = \vec{MO} + \vec{OP} = -R\alpha\vec{i}_{OC} + R(x_P\vec{i} + y_P\vec{j} + z_P\vec{k})$  and  $\vec{dl} = Rd\alpha\vec{i}_{OC}$  with  $\vec{i}_{OC} = \cos \psi_b\vec{i} + \sin \psi_b\vec{j}$ . Thus,  $\vec{k}(\vec{dl} \times \vec{MP}) = R^2(y_P \cos \psi_b - x_P \sin \psi_b)d\alpha$ .  $(\vec{MP})^2 = ((x_P - \alpha \cos \psi_b)^2 + (y_P - \alpha \sin \psi_b)^2 + z_P^2)R^2$  thus:

$$v'_{i_{blade}} = \frac{\Gamma'_{eff}}{4\pi} (y_P \cos \psi_b - x_P \sin \psi_b) \times \int_{\alpha=0}^{\alpha=r_v} \frac{d\alpha}{((x_P - \alpha \cos \psi_b)^2 + (y_P - \alpha \sin \psi_b)^2 + z_P^2)^{3/2}} \quad (18)$$

Now, let  $X(\alpha) = (x_P - \alpha \cos \psi_b)^2 + (y_P - \alpha \sin \psi_b)^2 + z_P^2$ . Developping, we have  $X(\alpha) = \alpha^2 - 2(x_P \cos \psi_b + y_P \sin \psi_b)\alpha + (x_P^2 + y_P^2 + z_P^2) = \mathcal{A}\mathcal{B}\alpha + \mathcal{C}\alpha^2$  for which notation, an expression of the above integral can be found as:

$$\int_{\alpha=0}^{\alpha=r_v} \frac{d\alpha}{X(\alpha)} = \frac{2}{\mathcal{Q}} \left( \frac{2\mathcal{C}r_v + \mathcal{B}}{\sqrt{X(r_v)}} - \frac{\mathcal{B}}{\sqrt{\mathcal{A}}} \right)$$

with  $\mathcal{Q} = 4\mathcal{A}\mathcal{C} - \mathcal{B}^2$  Thus, finally,

$$v'_{i_{blade}} = \frac{\Gamma'_{eff}}{4\pi} (y_P \cos \psi_b - x_P \sin \psi_b) \frac{2}{\mathcal{Q}} \left( \frac{2\mathcal{C}r_v + \mathcal{B}}{\sqrt{X(r_v)}} - \frac{\mathcal{B}}{\sqrt{\mathcal{A}}} \right) \quad (19)$$

with  $\mathcal{Q} = 4\mathcal{A}\mathcal{C} - \mathcal{B}^2$ ,  $\mathcal{C} = 1$ ,  $\mathcal{B} = -2(x_P \cos \psi_b + y_P \sin \psi_b)$ ,  $\mathcal{A} = x_P^2 + y_P^2 + z_P^2$  and  $X(r_v) = \mathcal{A} + \mathcal{B}r_v + \mathcal{C}r_v^2$  with  $\Gamma'_{eff} = \Gamma'(\frac{\rho^2}{1+\rho^2})$  and,

$$\rho^2 = \frac{(\vec{OP} \times \vec{i}_{OC})^2}{R^2 c_R^2}$$

$$\rho^2 = \frac{[(x_P \vec{i} + y_P \vec{j} + z_P \vec{k}) \times (\cos \psi_b \vec{i} + \sin \psi_b \vec{j})]^2}{R^2 c_R^2}$$

$$\rho^2 = \frac{[(x_P \sin \psi_b - y_P \cos \psi_b) \vec{k} + z_P \cos \psi_b \vec{j} - z_P \sin \psi_b \vec{i}]^2}{R^2 c_R^2}$$

$$\rho^2 = \frac{[(x_P \sin \psi_b - y_P \cos \psi_b)^2 + z_P^2]}{R^2 c_R^2}$$

#### 5.4 Radial averaging of downwash

The computation of the downwash along the blade involves occurrences of close blade vortex interactions. This may result in spurious variations of downwash dependent on radial grid definition and offset. To address this situation, a radially averaged expression of the downwash induced by the pairs of straight vortex line segments over a radial interval may be used.

The downwash induced by a straight vortex line segment at point B on point P situated on the blade is given from equation 15 as:

$$v'_B = -\Gamma' \frac{\rho^2}{1 + \rho^2} \frac{r_v p_B}{2\pi(z_{PB}^2 + p_B^2)} \frac{1}{(z_{PB}^2 + p_B^2 + r_v^2)^{1/2}}$$

with  $\Gamma'_{eff} = \Gamma'(\frac{\rho^2}{1+\rho^2})$  and  $\rho^2 = \frac{(p_B^2 + z_{PB}^2)}{c_R^2}$ . Let  $\mathcal{D} = z_{PB}^2 + c_R^2$  and  $\mathcal{E} = z_{PB}^2 + r_v^2$ . Then,

$$v'_B = -\frac{\Gamma' r_v}{2\pi} \frac{p_B}{(p_B^2 + \mathcal{D})(p_B^2 + \mathcal{E})^{1/2}} \quad (20)$$

For an angle  $\beta$  between the vortex segment and the blade, the downwash expression at the control point P is averaged over the projected length  $\Delta r' = |\Delta r \sin \beta|$  where  $\Delta r$  is the averaging distance, and  $\beta = \Phi_v - \psi_P$  where  $\Phi_v$  is the azimuth angle of the straight vortex line segment, ( $\Phi_v = \arg i_{AC}$ ) Thus:

$$\bar{v}'_B = -\frac{\Gamma' r_v}{2\pi \Delta r'} \int_{p_B - \Delta r'/2}^{p_B + \Delta r'/2} \frac{p_B dr}{(p_B^2 + \mathcal{D})(p_B^2 + \mathcal{E})^{1/2}} \quad (21)$$

Reference [1] provides the expression resulting from this integral:

$$v'_B = -\frac{\Gamma' r_v}{2\pi 2k \Delta r'} \ln \left[ \frac{(p_{B_2}^2 + \mathcal{E})^{1/2} - k (p_{B_1}^2 + \mathcal{E})^{1/2} + k}{(p_{B_2}^2 + \mathcal{E})^{1/2} + k (p_{B_1}^2 + \mathcal{E})^{1/2} - k} \right] \quad (22)$$

where  $p_{B_1} = p_B - \Delta r'/2$ ,  $p_{B_2} = p_B + \Delta r'/2$ ,  $k = (\mathcal{E} - \mathcal{D})^{1/2} = (r_v^2 - c_R^2)^{1/2}$ , and  $\mathcal{D} = z_{PB}^2 + c_R^2$ ,  $\mathcal{E} = z_{PB}^2 + r_v^2$ .

## 6 Positioning of the vortex elements

For each spiral turn trailed by all blades, the position of the two points B have to be known by the age of the vortex element they are at so that  $p_B$ ,  $z_{PB}$ ,  $\Phi_v$  which are necessary for the computation of induced velocities can be computed.

The original method involves an empirical formula used for the location of the critical elements of the trailing vortex system . However, its implementation involves the use of an extra remainder term for the induced velocity computation as specified in reference [1] due to a discontinuity in the formulation. Its implementation also revealed it to be unsuitable for points where the induced velocity is wanted outside the blade and/or outside the tip path plane . The method chosen for its simplicity and absolute reliability in all cases is an iteration method by dichotomy of each spiral turn where the two points B are to be found. The criteria for convergence is expressed in terms of the angle between the projection on the tip path plane of  $\vec{PB}$  and  $\vec{j}_{AC}$  which, in absolute value is ascribed to be smaller than 3 degrees. The algorithm first advances along the spiral turn in increments of sixty degrees until the above angle changes sign. Then, on the interval thus located, a dichotomy process is performed until the tolerance in angle is achieved. The other point B is then found on the remaining portion of the spiral turn in the same way. Let a step be defined as a computation of the angle between the projections of  $\vec{PB}$  and  $\vec{j}_{AC}$ , that is, either after an increment along the spiral turn or in a division of the interval where there is a change of sign. With the increment of sixty degrees chosen, the number of steps necessary for convergence for each point has been minimized to six, in average. The advantage of this method is a simplified algorithm, with an adjustable tolerance of positioning of the critical elements, at the same amount of computation time as the original method. No discontinuity effects are brought in by the algorithm, and thus the need for the extra remainder term is eliminated. However, the main reason for this algorithm is that the original one could not handle accurately, points outside the blade, even after extensive modification.

## 7 Development of the code

The development was done in two phases. The first phase saw the experimentation with the original scheme as presented in reference [1]. The limitations of the graphic capabilities of the software available at that time did not allow efficient separation of the graphics programming and the computation coding. Also, some of the graphics work had to be done on another system where more advanced software was available. As soon as adequate software became available on the system to be used on a permanent basis, coding of the second version of the scheme took place, by taking care of separating the computation core of the code from the pre and post processing of the computation. In addition, the modularity of the wake model methodology was respected by separating code

modules relative to the computation of the critical locations in the trailing vortex system from those relative to the induced velocity computation. Thus, three core modules were created, each compilable, testable independantly and from which, validating graphics can be generated: The first module finds the critical locations in the tip path plane of the trailing vortex system . The second module comprises the subroutine computing the momentum values of induced downwash as well as the vertical distorted geometry of the trailing vortex system . Then the third module comprises the computation of the induced velocity at a given point. The first two modules are tested through one program each, generating graphics shown in Figure 1 and 2, respectively. The third module which involves computation of induced velocity components is numerically tested through the debugger of the compiler. In addition, this last module is used by two front-end programs producing the numerical results and generating the plots associated with those results. The first program computes the induced downwash seen by one rotating blade along its span. Figure 3 represents a plot obtained through this program. The second program computes the induced downwash field over regions of the rotor disc. This program produces both three dimensional and contour plots of the results as illustrated by Figure 4 and 5. All programs use the same input file and can be linked and run together or at various degrees of independance. The variable names fully use the capability of the compiler to recognize long names which are directly analogous to those used in the report for good readability of the code.

## 8 Results

The test case treated is the same as the one treated in reference [5]. It is a four bladed rotor, at an angle of attack of -3 degrees for an advance ratio  $\mu_x = .15$ . From this, a climb ratio  $\mu_z = V \sin \alpha / \Omega R$  was computed. The test data is thus summarized below:

- $b = 4$
- $C_T = .0064$
- $\mu_x = .15$
- $\mu_z = -.0078$

Other input data include the position of the point above the tip path plane where the induced downwash is wanted, the vortex core radius, the contracted radius and the number of turns used for the trailing vortex system of each blade.

- $z_P = .077$
- $c_R = .077$

- $r_v = 1$ .
- $N = 3$

The computation time is of the order of one half second per point where the induced velocity by the trailing vortex system is computed. No first harmonic variation of circulation was used in the computation of induced downwash. Thus, blade bound vorticity induced downwash averages out over time.

- Figure 1 shows the critical locations in the trailing vortex system as seen in projection in the tip path plane for a point P outside the rotor disc.
- Figure 2 shows the geometry of the distorted trailing vortex system as seen in perspective from downstream.
- Figure 3 shows the plot of the induced downwash seen by a rotating blade from azimuth  $\psi_r$  of 0 to 360 degrees along the span from .2 to 1.2 radial position (non dimensionalized by  $R$ ). The results are given in term of  $\lambda_i^*$ , reduced induced inflow ratio, ( $\lambda_i^* = \lambda_i / \lambda_{i,0H}$ ) where  $\lambda_i$  is the induced inflow ratio, ( $v / \Omega R$ ) and  $\lambda_{i,0H}$  is the momentum value of induced inflow ratio at hover ( $-\sqrt{C_T/2}$ ). Thus, a positive value corresponds to an induced downwash and a value of 1 corresponds to  $\lambda_i^* = \lambda_{i,0H} = -\sqrt{C_T/2} = -.056$ . The option of radially averaged induced velocity was used for this case producing smoother results than with the simpler expression.
- Figure 4 shows the plot of the induced downwash field on the region of azimuth 0 to 360 degrees along a radial position from .2 to 1.2 (non dimensionalized by  $R$ ). It can be seen that this plot is very similar to that of the induced downwash seen by a rotating blade but it is smoother.
- Figure 5 shows the contour plot of the induced downwash field on the region of azimuth 0 to 360 degrees along a radial position from .2 to 1.2, (non dimensionalized by  $R$ ). This plot contains the same information as the preceding plot. induced downwash seen by a rotating blade but it is smoother. Overall, there is a good agreement of the magnitude of the induced downwash with the experimental results obtained in reference [5]. The trends are followed reasonably well on the retreating side and the leading edge with a region of upwash extending from 160 to 270 degrees. The trends are not followed well at the trailing edge and advancing side.

## 9 Conclusion

The test case computed with the present scheme shows disagreements with experimental results obtained in reference [5]. Interesting results can otherwise be observed as to the similarity of instantaneous induced downwash seen by a

rotating blade and induced downwash field plots. Different options and parameter values can be used to study their influence on the results obtained. Among those possibilities are:

- Utilization of radial averaging and the variation of the averaging interval used.
- Variation of vortex core radius  $C_R$
- Introduction of first harmonic variation of circulation strength over the trailing vortex system and on the blade bound vorticity.
- Variation of the contracted radius  $r_v$
- Variation of the number of trailing vortex system turns taken into consideration
- Variation of the number of increments over which, the induced downwash is averaged over azimuth (The present number is 10).

It is not fully known yet, however what the importance of a shed vortex system is and whether it should be added to this scheme. Other factors entering into consideration might be lifting surface effects, inboard trailing wake system and presence of a body as is the case for the experimental case in reference [5]. In conclusion, various options and parameters' influence on the results can be investigated with the present model and may lead to useful interpretations and better agreement with experimental data.

## References

- [1] Beddoes T.S., Westland Helicopters Ltd. A wake model for high resolution airloads.
- [2] Heyson H.H., Katzoff S. Induced velocities near a lifting rotor with nonuniform disk loading. NACA Report 1319, 1956.
- [3] Egolf T.A., Landgrebe A.J. Generalized wake geometry for a helicopter rotor in forward flight and effect of wake deformation on airloads. A.H.S. Annual Forum 1984.
- [4] Scully M.P. Computation of helicopter rotor wake geometry and its influence on rotor harmonic airloads. ASRL TR178-1, 1975.
- [5] Berry J.D., Hoad D.R., Helliott J.W., Althoff S.L. Helicopter rotor induced velocities theory and experiment. Rotorcraft Aerodynamics Office. Aerostructures Directorate, USAARTA-AVSCOM, Langley Research Center, Hampton, Virginia. Presented at the AHS Specialists' Meeting on Aerodynamics and Aeroacoustics, Arlington, Texas, February 25-27, 1987.

# TIP Plan View

$b = 4$   
 $\mu_s = 0.150$   
 $\mu_r = -0.00780$   
 $c_t = 0.00640$

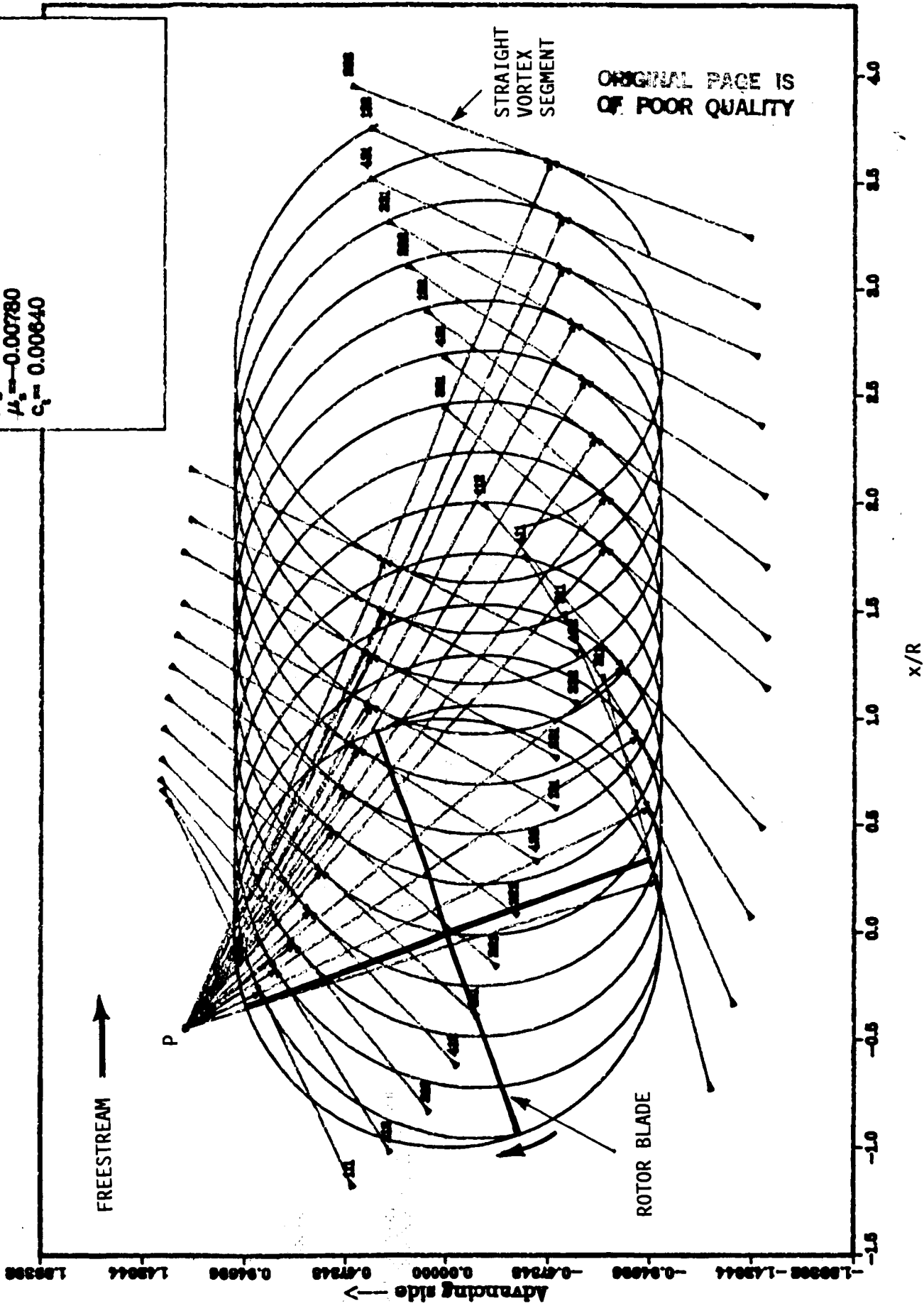


Figure 1: Critical locations in the trailing vortex system as seen in projection in the tip path plane for a point P outside the rotor disc.

WAKE VIEW

ORIGINAL PAGE IS  
OF POOR QUALITY

$b = 4$   
 $\mu_2 = 0.150$   
 $\mu_1 = -0.00780$   
 $c_1 = 0.00640$

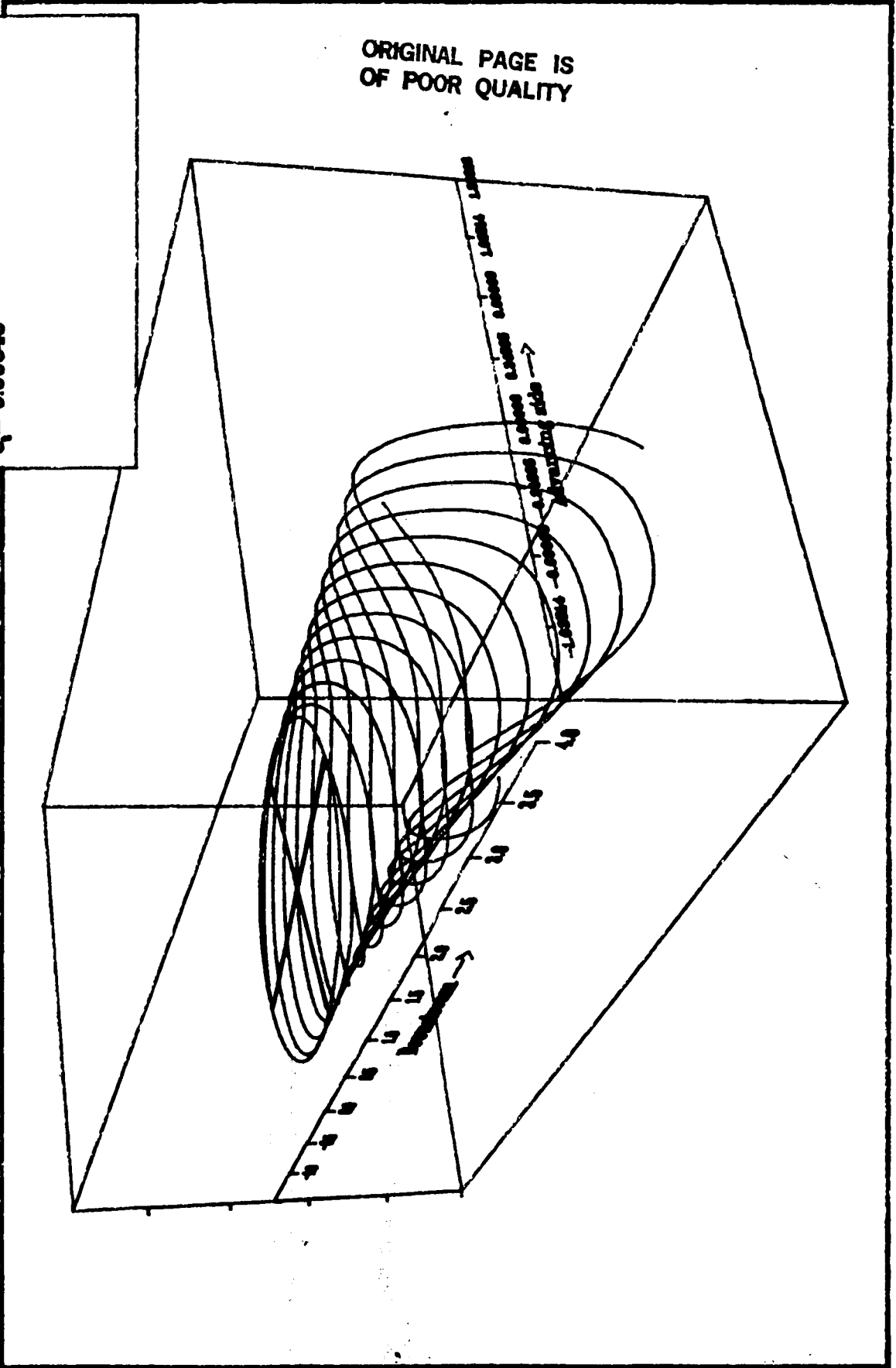


Figure 2: Perspective view from downstream of the distorted tip vortex system.

$b = 4$   
 $\mu_x = 0.150$   
 $\mu_y = -0.00780$   
 $C_x = 0.00640$   
 $C_y = 0.07700$

ORIGINAL PAGE IS  
OF POOR QUALITY

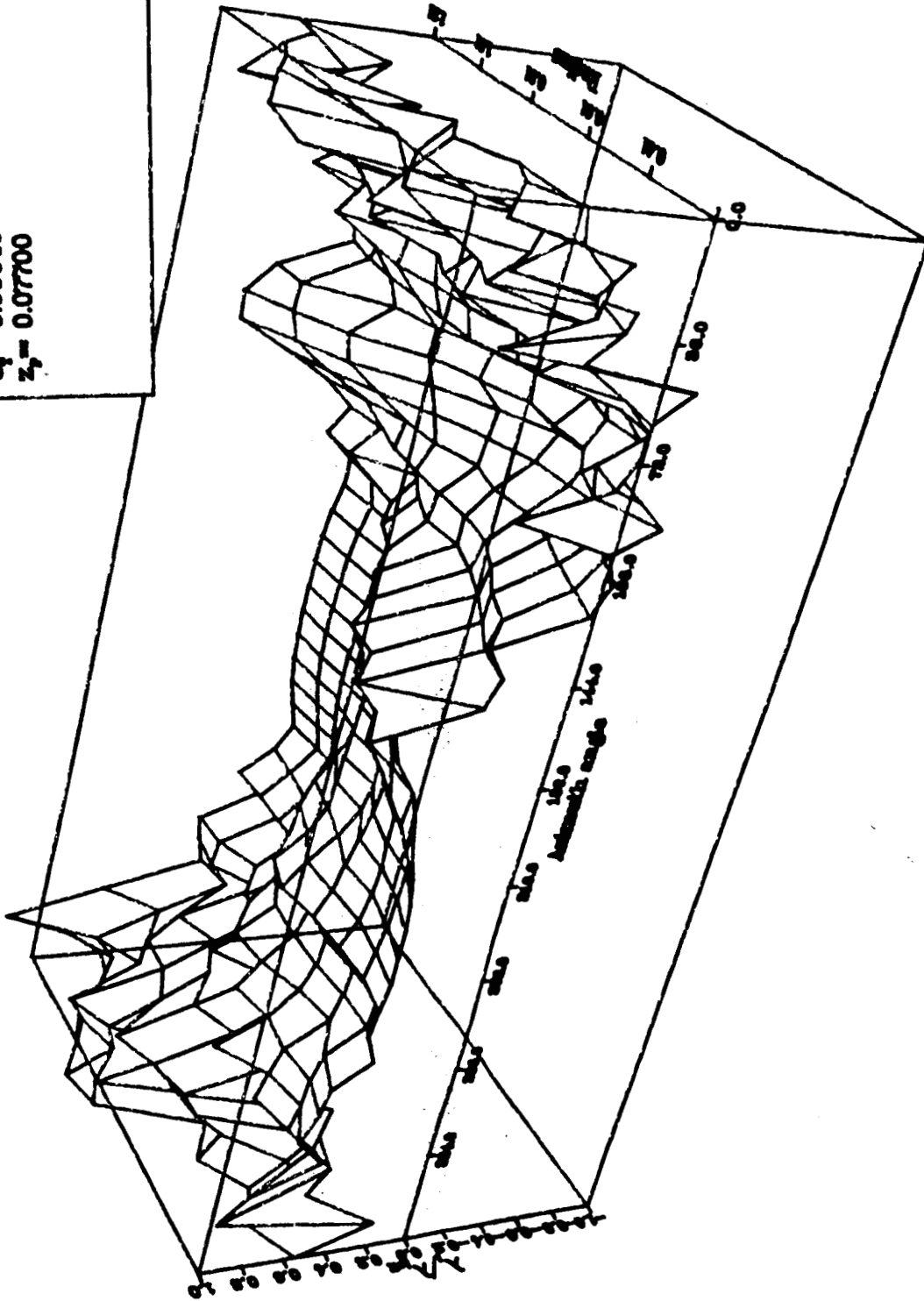


Figure 3: Azimuthal variation of the spanwise distribution of induced downwash, as seen by a rotating blade. The downwash is normalized using the momentum-theory value of induced velocity under hover conditions. Radial averaging has been used to smooth out discontinuities due to discretization in the proximity of vortices.

INDUCED DOWNWASH FIELD

$b = 4$   
 $\mu_1 = 0.150$   
 $\mu_2 = 0.00780$   
 $C_1 = 0.00840$   
 $\alpha_1 = 0.07700$

ORIGINAL PAGE IS  
OF POOR QUALITY

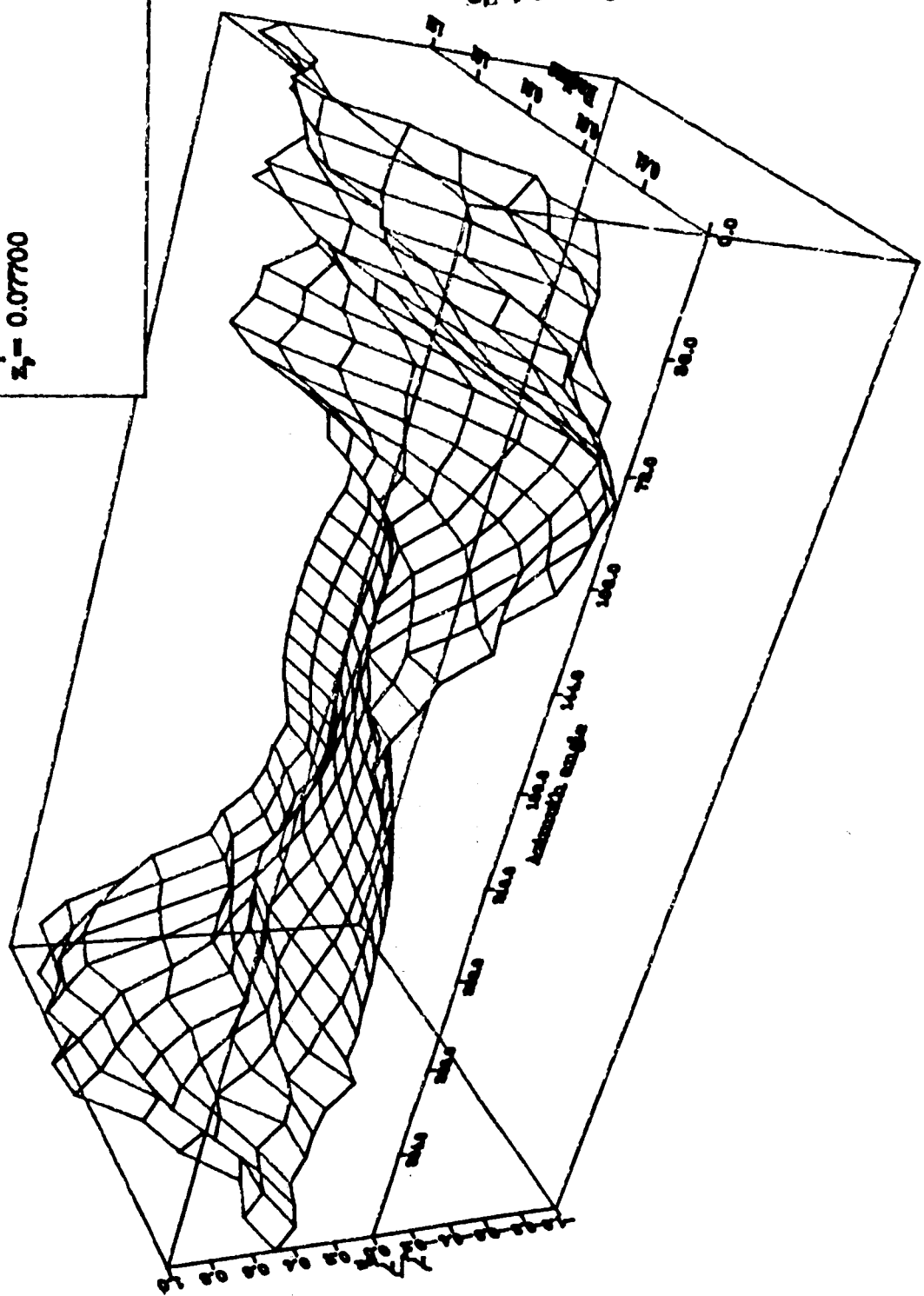


Figure 4: Azimuthal distribution of induced downwash in the non-rotating reference frame.

# Induced downwash field

$b = 4$   
 $\mu_x = 0.150$   
 $\mu_y = -0.00780$   
 $C_x = 0.00640$   
 $C_y = 0.07700$

ORIGINAL PAGE IS  
OF POOR QUALITY

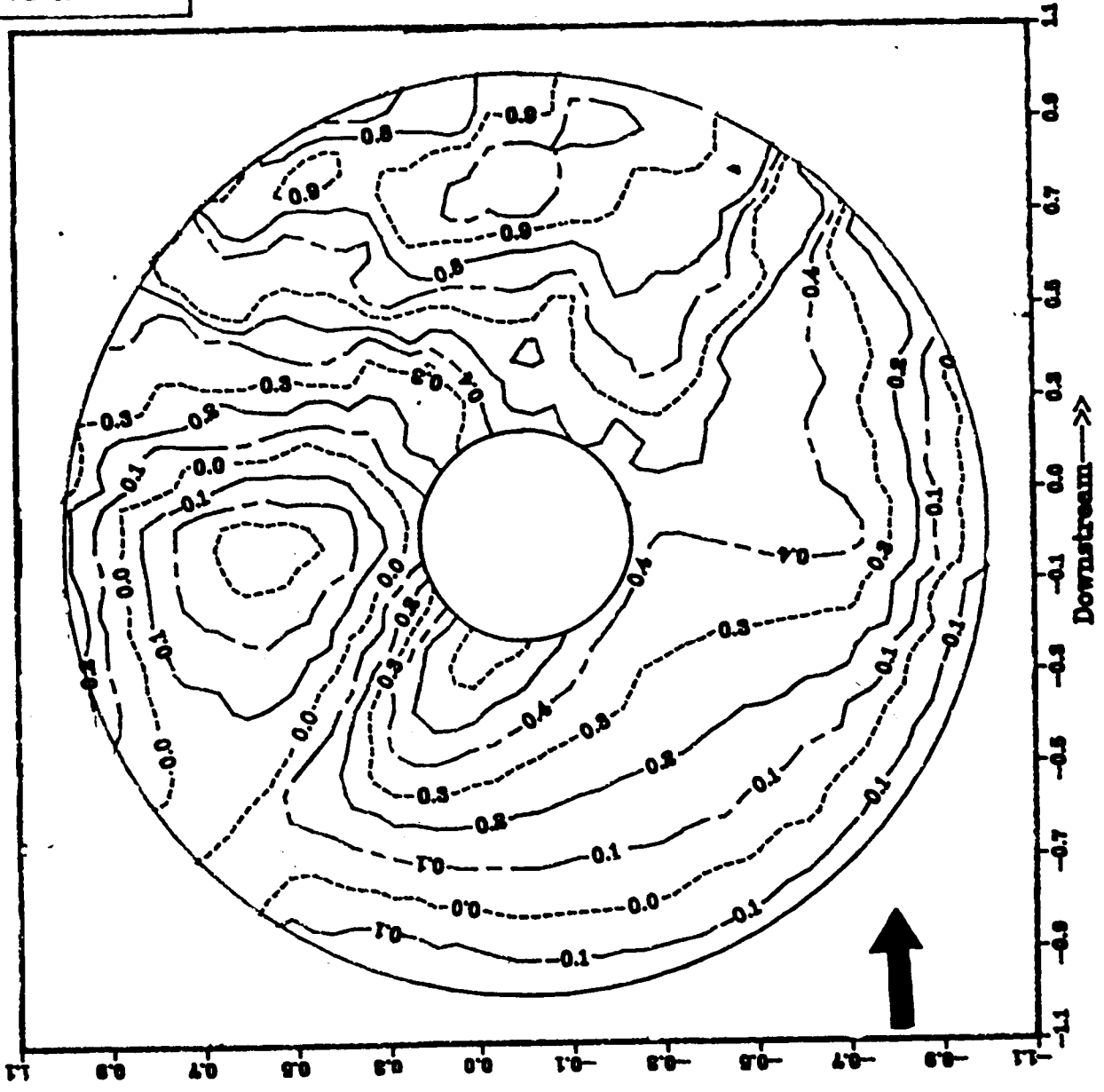


Figure 5: Contour plot of the induced downwash field in the non-rotating reference frame.